Topological defects in a two-dimensional liquid crystal confined in a circular nanocavity

D. de las Heras[*]

Departamento de Física Teórica de la Materia Condensada, Universidad Autónoma de Madrid, E-28049 Madrid, Spain

E. Velasco[†]

*Departamento de Física Teórica de la Materia Condensada and Instituto de Ciencia de Materiales Nicolás Cabrera,
Universidad Autónoma de Madrid, E-28049 Madrid, Spain*

L. Mederos[‡]

Instituto de Ciencia de Materiales de Madrid, Consejo Superior de Investigaciones Científicas, E-28049 Madrid, Spain

Using a microscopic theory based on excluded-volume interactions, we analyze the structure and thermodynamic stability of configurations in a two-dimensional liquid crystal confined into a (small) circular nanocavity. Weak homeotropic anchoring conditions are considered, and topological defects of total charge $k=+1$ are discussed. It is found that, for small cavity radii, the cavity is free of defects at the expense of surface free energy not being optimized. For larger cavities, a configuration with two repulsive $k=+1/2$-charge point defects is always stable. The two configurations are equally stable thermodynamically (structural or Frederiks transition) on a curve in the chemical potential-cavity radius plane. This curve ends for chemical potential and cavity radius below some critical values. Elastic-theory arguments are used to explain the stability of the defected structure compared with the one free of defects. Our results indicate that the two-defect structure is always more stable than the one with a single point defect of charge $k=+1$ at the cavity center, which, in agreement with computer simulation, is never found to be stable. Finally, the relation with the bulk behavior of the fluid is discussed.

I. INTRODUCTION

Topological defects in liquid crystals continue to attract interest from many perspectives. One of them is obviously related to the important technological applications of liquid crystals [1] and the role of defects in display-cell operation and the design of new technologies [2]. More recent studies have unveiled the implications of this topic in cosmology [3]. In three-dimensional (3D) nematics, both line (disclination) and point (monopole) defects are possible, while only the point defects can be obtained in two-dimensional (2D). A defect is a singularity of the nematic director field [4] characterized by a topological charge, i.e., the number of turns of the director when the singularity is completely encircled. The Frank-Oseen [5] elastic theory has been extensively used to study defects in liquid crystals. It assumes smooth variations in the director in space and therefore is not able to account for the structure in the immediate neighborhood of the singularity. The description of strong variations in fluid properties near defects is usually made with phenomenological theories of the Landau–de Gennes type, containing effective phenomenological parameters, and based on a local ordering tensor $Q(r)$ [1]. Many applications of Landau–de Gennes theories to line and point defects also exist in the literature. However, phenomenological theories lack any connection with particle shape and particle interactions. Simulations of

lattice models [6], and more recently of continuous particle models [7–10], have been done recently to fill this gap, but there is a lack of theoretical models based on microscopic particle interactions, which can consistently deal with the thermodynamic and structural aspects of the problem in a less computational demanding way.

In this paper we apply the density-functional theory to study the thermodynamics and structural properties of point defects in a 2D nematic liquid confined into a (small) circular nanocavity. The two-dimensional geometry is used because of computational limitations, but the two-dimensional case is interesting by itself, and we are not meaning to approximate the most straightforward 3D (cylindrical) geometry by the present 2D calculations. The method based on density-functional theory could, in principle, be applied to 3D cavities and other topologies. The 2D cavity is an interesting setup since there exists the possibility that defects, i.e., configurations with a net topological charge, may be stabilized as a result of the frustrating boundary. Here the stability of defects results from the competing effects of surface elastic and defect core energies: for the fluid to optimize the surface energy, one or more point defects must necessarily appear in the cavity.

We restrict ourselves to studying relatively small nematic cavities (nanocavities), of only a few particle lengths in diameter, which is an interesting problem as the nanoconfinement will, in general, induce severe structural constraints that can lead to new phenomena. Homeotropic, i.e., perpendicular to the surface, orientation of the nematic director is assumed to be energetically favored at the surface, but this condition is weak in the sense that other terms in the free energy can overcome the favored surface configuration. The

————————

[*]daniel.delasheras@uam.es
[†]enrique.velasco@uam.es
[‡]l.mederos@icmm.csic.es

total topological charge in the cavity is $k=+1$. This can be obtained from a single defect at the center or from two $k=+1/2$ defects symmetrically situated with respect to the center. Alternatively, when the surface energy is relatively unimportant compared to other energies, the fluid may get rid of the defects in the cavity and adopt a more or less uniform director configuration by not optimizing the surface energy. We are interested in the relative stability of these structures, the ones with a net topological charge and that with null charge, and a phase diagram describing the stability of the different structures is predicted. Note that our theoretical approach allows us to treat, in a consistent way, the effect of thermodynamic variables, chemical potential (or temperature), and radius of the cavity on this stability. In particular, we will discuss the relation between the defect structure in the cavity and the bulk isotropic-nematic transition. Two-dimensional defects have not received much theoretical attention so far, most studies being devoted to the structure of 3D defects. With few exceptions (see, e.g., [11]), the effect of thermodynamic conditions has been ignored. For example, phase diagrams for 3D nematic droplets and cylindrical pores were obtained by Kralj and Žumer [12] using a simplified Landau–de Gennes theory. Conditions were intentionally chosen to be far from the bulk transition, and the nematic order parameter was assumed to be uniform. Consequently only the effect of surface and bulk fields on the different director configurations was investigated.

By contrast, the theoretical point of view adopted here is based on a microscopic theory, i.e., density-functional theory, which explicitly incorporates particle interactions. This is a step beyond classical treatments based on mesoscopic theories and provides a theoretical description intermediate between mesoscopic approaches and computer simulation studies. One of its advantages is that the elastic constants (in particular, the problematic surface elastic constants) and other phenomenological parameters do not appear explicitly in the theory but only implicitly through the interactions and distribution functions in a free-energy functional which is minimized. The defect core appears naturally, and this is ideal when studying nanocavities, as in this case the contribution of defects cannot be ignored, as is usually the case in larger-sized nematic droplets treated with elastic theories.

Even though our theory is mean field, we have access to density and orientational order-parameter inhomogeneities, all coupled consistently with the local director and the surface contributions. As one of the outcomes of this investigation, we found a very weak structure of the fluid in the cavity, as a result of the high degree of confinement and the existence of frustration in the nematic field (i.e., defects have a disordering effect [11]). We also show the structure of the defect cores and study the energetics associated with the defect position within the cavity. For instance, we conclude that the radial nematic configuration, with a single point defect of charge $k=+1$ at the center, is always unstable with respect to a configuration with two $k=+1/2$-charge defects. This is in agreement with simulation results [9,10]. In turn, for the type of surface considered, we find competition between this structure and the structure containing no defects.

After explaining the density-functional model in detail and some technical issues concerning the numerical ap-
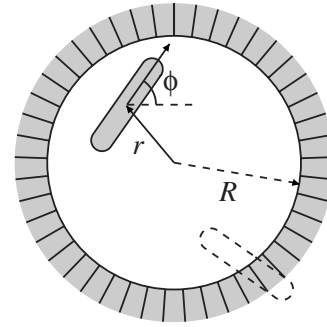

FIG. 1. Schematic of the cavity. r is the position vector of a particle, while ϕ is the angle of its long axis with respect to the x axis. R is the radius of the cavity. Particle drawn with dashed line has its center of mass right at the wall surface.

proach in Sec. II, we present the results in Sec. III. First we review the bulk properties in Sec. III A and then the structure and thermodynamics of the confined fluid in Sec. III B. A short discussion on links with elastic theory is given in Sec. III C, while Sec. III D provides some data which suggest the existence of scaling properties in the configuration with two $k=+1/2$ defects with respect to the cavity radius, and the relation with the bulk isotropic-nematic transition is discussed in Sec. IV. Finally, Sec. V is devoted to providing some conclusions of the work.

II. THEORY

The particle model used here is the two-dimensional version of the popular spherocylinder model, i.e., a hard discorectangle (HDR), Fig. 1. These particles consist of a rectangular part, length L and width D, and two semicircular caps of diameter D at the two opposite ends of the rectangle. The interactions between these hard particles will be exclusively excluded-volume interactions since these interactions are sufficient to generate nematic ordering. This means that the relevant thermodynamic intensive variable will be the chemical potential rather than the temperature. The HDR particles will be placed inside a circular cavity of small radius R (Fig. 1).

A. Density-functional theory

The statistical mechanics of this system was treated using density-functional theory, which is focused on the one-particle distribution function $\rho(r, \phi)$, where r is the location of the particle center and ϕ the angle of the particle axis with respect to the laboratory-frame x axis (Fig. 1). We write $\rho(r, \phi)=\rho(r)f(r, \phi)$, where $f(r, \phi)$ is the angular distribution function, and the average local density is $\rho(r)=\int d\phi \rho(r, \phi)$. As usual, we split the free-energy functional into ideal excess and external parts,

$$F[\rho] = F_{id}[\rho] + F_{exc}[\rho] + F_{ext}[\rho], \tag{1}$$

with

$$\beta F_{id}[\rho] = \int_A d\mathbf{r} \rho(\mathbf{r}) \left\{ \log\left[\frac{\rho(\mathbf{r})\Lambda^2}{2\pi}\right] - k^{-1} S_{rot}(\mathbf{r}) \right\}, \quad (2)$$

where A is the total area of the cavity, Λ is the thermal wavelength, and $S_{rot}(\mathbf{r})$ is the local rotational entropy density,

$$S_{rot}(\mathbf{r}) = -k \int_0^{2\pi} d\phi f(\mathbf{r},\phi) \log[2\pi f(\mathbf{r},\phi)]. \quad (3)$$

As usual, $\beta = 1/kT$, k being Boltzmann's constant. The factors 2π in the arguments of the logarithms in Eq. (2) and (3) are introduced so as to make $S_{rot}=0$ when particles are orientationally disordered, i.e., when $f(\mathbf{r},\phi)=1/2\pi$.

The excess part can be written in terms of that of a reference system. The reference system used will be a fluid of locally parallel hard ellipses since this fluid can be exactly mapped onto a fluid of hard disks and there are very accurate theories for the thermodynamics of this system. The hard ellipse chosen will have the same particle area v_0 and the same aspect ratio as the HDR: if $\sigma_\parallel$ and $\sigma_\perp$ are the diameters of the ellipses along the major a minor diameters and σ_e is the effective diameter of the reference hard disk, with $\sigma_e^2 = \sigma_\parallel \sigma_\perp$, then we demand

$$\begin{cases} \dfrac{L+D}{D} = 1 + \chi = \dfrac{\sigma_\parallel}{\sigma_\perp} \\ \dfrac{\pi D^2}{4} + LD = \dfrac{\pi}{4}\sigma_\parallel \sigma_\perp = \dfrac{\pi}{4}\sigma_e^2. \end{cases} \quad (4)$$

In the following we will use $\chi \equiv L/D = 15$, which gives $L = 3.346\sigma_e$ and $D = 0.223\sigma_e$. The thermodynamics of the fluid of parallel hard ellipses or of the fluid of hard disks can be described from the equation of state $p(\eta)$, where p is the pressure and

$$\eta = \frac{\pi\rho}{4}\sigma_e^2 = \frac{\pi\rho}{4}\sigma_\parallel \sigma_\perp \quad (5)$$

is the packing fraction. For the equation of state of hard disks we have used one of the approximations proposed by Baus and Colot [13] (specifically their Z_2 expression), which gives very good results in the fluid range. The explicit expression for the excess free energy per particle of the uniform fluid is

$$\beta\Psi_{exc}(\eta) = (c_2+1)\frac{\eta}{1-\eta} + (c_2-1)\log(1-\eta), \quad (6)$$

with

$$c_2 = \frac{7}{3} - \frac{4\sqrt{3}}{\pi} \simeq 0.1280. \quad (7)$$

The excess free energy is then written as

$$F_{exc}[\rho] = \int_A d\mathbf{r} \int_0^{2\pi} d\phi \rho(\mathbf{r},\phi)\varphi(\mathbf{r},\phi), \quad (8)$$

where the local excess free energy per particle is

$$\varphi(\mathbf{r},\phi) = \frac{\Psi_{exc}[\eta(\mathbf{r})]}{\pi\sigma_e^2 \rho(\mathbf{r})}$$

$$\times \int_A d\mathbf{r}' \int_0^{2\pi} d\phi' \rho(\mathbf{r}',\phi') v_{exc}(\mathbf{r}-\mathbf{r}',\phi,\phi'),$$

$$(9)$$

where v_{exc} is the overlap function of two HDR particles (equal to zero if particles overlap and unity otherwise). Note that when $\rho(\mathbf{r},\phi)$ is a constant, $\varphi = \Psi_{exc}$. Finally, the contribution from the external potential is

$$F_{ext}[\rho] = \int_A d\mathbf{r} \int_0^{2\pi} d\phi \rho(\mathbf{r},\phi) v_{ext}(\mathbf{r},\phi). \quad (10)$$

The external potential is simply taken to be a hard wall acting over the particle centers of mass:

$$\beta v_{ext}(\mathbf{r},\phi) = \begin{cases} \infty, & r > R \\ 0, & r < R. \end{cases} \quad (11)$$

Here r is the radial distance measured from the center of the cavity (Fig. 1).

It is convenient to define a connection between the distribution function $f(\mathbf{r},\phi)$ and the order tensor. This connection will be established via a local nematic order parameter q and a local director given by its polar angle Ψ (in 2D the order tensor only has one nontrivial eigenvalue, hence a single order parameter; therefore there is no biaxiality in 2D, in contrast with the 3D case). To simplify the calculations, we consider a parametrization for the angular dependence of $f(\mathbf{r},\phi)$. The simplest choice that respects the basic symmetry of the angular distribution [for our particles with head-tail symmetry $f(\mathbf{r},\phi)=f(\mathbf{r},\phi+\pi)$] is

$$f(\mathbf{r},\phi) = \frac{e^{\alpha(\mathbf{r})\cos 2[\phi-\Psi(\mathbf{r})]}}{\displaystyle\int_0^{2\pi} d\phi e^{\alpha(\mathbf{r})\cos 2[\phi-\Psi(\mathbf{r})]}}, \quad (12)$$

where the field $\Psi(\mathbf{r})$ is the local tilt angle of the nematic measured with respect to the x axis, and $\alpha(\mathbf{r})$ is a variational function related with the local nematic order parameter $q(\mathbf{r})$ by

$$q(\mathbf{r}) = \int_0^{2\pi} d\phi f(\mathbf{r},\phi)\cos\{2[\phi-\Psi(\mathbf{r})]\}. \quad (13)$$

This equation establishes a one-to-one correspondence between $\alpha(\mathbf{r})$ and $q(\mathbf{r})$. Now, within this approximate scheme, the full description of the liquid crystal in terms of the density $\rho(\mathbf{r},\phi)$ can be given, in a completely equivalent way, by the set of functions $\{\rho(\mathbf{r}), q(\mathbf{r}), \Psi(\mathbf{r})\}$. In the following we will use the local packing fraction, $\eta(\mathbf{r})$, given by Eq. (5), instead of the local density $\rho(\mathbf{r})$, as a basic density variable.

Now our cavity of finite area A is coupled to a thermal and particle reservoir at temperature T and chemical potential μ, with which the cavity is assumed to interchange energy and particles (the exact particle interchange mechanism need not concern us now; the cavity could be experimentally realized, e.g., by filling a circular indentation on a surface,

thus producing a finite quasimonolayer, which could be in contact with a semi-infinite fluid above). The equilibrium configuration of the cavity at fixed (μ, A, T) will be obtained by minimization of the cavity grand potential functional $\hat{\Omega}[\rho]$:

$$\hat{\Omega}[\rho] = F[\rho] - \mu \int_A d\mathbf{r} \int_0^{2\pi} d\phi \rho(\mathbf{r}, \phi) \quad (14)$$

with respect to variations in the variables defined above. The average number of particles $\bar{N}$ inside the cavity will be obtained by integration of the equilibrium density distribution $\rho(\mathbf{r})$ over the area A. In the results to be presented below $\bar{N} \sim 10^2 - 10^3$ so that the cavity is a small system, far from the thermodynamic limit. Alternatively we can minimize the Helmoltz free-energy functional $F[\rho]$ at fixed number of particles N; the results would be equivalent, provided care is taken to correctly identify the chemical potential [14]. In the limit of large cavities we would recover bulk behavior.

B. Numerical details

To obtain the functional minimum of the free energy, we first discretized the two-dimensional space xy into a square lattice with spacing $\Delta x = \Delta y = 0.089\sigma_e$, with mesh points (x_i, y_j). This represents 40 points in a particle length $L + D$. Obviously the circular surface was approximated by a zigzag line. However, the mesh spacing is fine enough for the approximation to be accurate, as will be demonstrated by the density and order-parameter profiles to be presented below. The spatial integrations were calculated using the trapezoidal rule, while the angular integrals were approximated using Gaussian quadrature with 30–40 roots. The density distribution, expressed in terms of the set $\{\eta(\mathbf{r}), q(\mathbf{r}) \text{ and } \Psi(\mathbf{r})\}$, was discretized as η_{ij}, q_{ij}, and Ψ_{ij}, and the free-energy functional was minimized using the conjugate-gradient method.

The structure of the liquid crystal inside the circular cavity has a high degree of symmetry. This symmetry has been used to simplify the calculations which, taking into account all the possible structures within the cavity (see Sec. III B), can be reduced to just one quadrant of the circle. In particular, the gradients of the discretized functional were calculated in this quadrant only.

III. RESULTS

A. Bulk behavior

First we present the results for the bulk phase transition. The HDR model has been studied by Monte Carlo (MC) computer simulation [15]. For aspect ratios χ larger than $\simeq 6$ a nematic phase seems to be stable. The transition appears to be continuous, of the Kosterlitz-Thouless type. Therefore, we would expect our mean-field functional to predict a continuous transition from the isotropic ($q = 0$) to the nematic ($q \neq 0$) phase. This is indeed the case. In Fig. 2(a) we compare the results for the pressure-density equation of state with the results from MC simulation. Overall the agreement is good. The arrow indicates the location of the continuous transition, which takes place at $\eta_{IN} = 0.257$ (quite close to the result
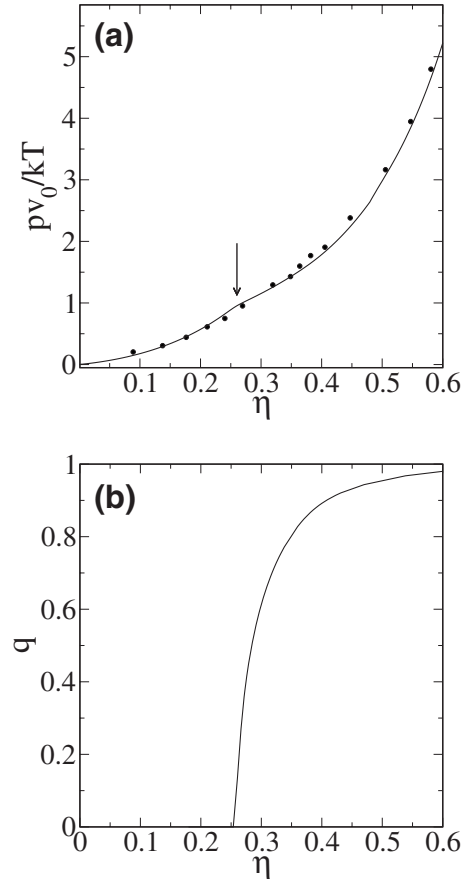

FIG. 2. (a) Equation of state (reduced pressure vs packing fraction) of a fluid of HDR with aspect ratio $\chi = 15$. Symbols are simulation data of Bates and Frenkel [15]. Continuous line is the result from density-functional theory. Arrow indicates packing fraction at which nematic phase bifurcates from isotropic phase. (b) Nematic order parameter as a function of packing fraction for the same system as in (a).

from scaled-particle theory, $\eta_{IN} = 0.248$) and at a reduced pressure $pv_0/kT = 0.98$. Estimates from simulation give $\eta_{IN} = 0.363$, a much higher value. Nevertheless, the simulations show strong system-size dependence of the nematic order parameter, as corresponds to a phase with quasi-long-range nematic order. Figure 2(b) shows the nematic order parameter as obtained from the density-functional theory. As expected, the order parameter becomes nonzero abruptly at the second-order phase transition.

Having obtained the bulk thermodynamic properties of the fluid, we now turn to the confined fluid and study its thermodynamic behavior and structural quantities: density, order-parameter, and director fields.

B. Phase behavior of confined fluid

The external potential [Eq. (11)] is known to favor a homeotropic (i.e., perpendicular to the wall) orientation of the fluid next to a flat wall. This has been shown in three dimensions using density-functional theory [18] and also in two dimensions by simulation [9]. Our present calculations indeed show this to be the case for the present setup. The
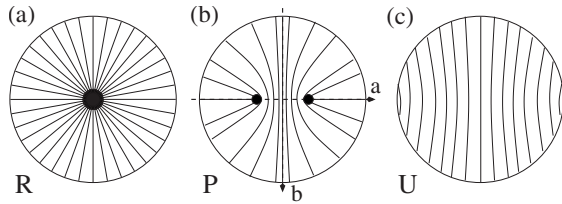
FIG. 3. Schematic of possible structures for the director field inside a circular cavity with homeotropic anchoring conditions. (a) Radial, R, configuration with a central point defect of charge $k=+1$. (b) Polar, P, configuration with two repulsive point defects of charge $k=+1/2$. (c) Uniform, U, configuration with the director approximately uniform in the whole cavity. "a" and "b" define two perpendicular diameters, the first along the defect line.

reason is that, even though the potential is neutral with respect to the orientation of a single particle, the favored orientation of a *dense* layer of adsorbed particles is homeotropic since in this way the free area per particle (including coupled surface and particle exclusion) is maximized. Note that the surface does not impose any specified values on density or order parameters, i.e., the surface does not act as a boundary condition in the model: the fluid will pay a free-energy cost in case the homeotropic orientation were not favored, and the surface values will result consistently from the theory. However, if this surface condition is perfectly satisfied, the defects have necessarily to be created in some regions of the cavity. The only way the fluid has to avoid the formation of defects is by not completely satisfying the homeotropic orientation at and near the surface.

From the previous discussion, we may think of three possible structures in the small-radius cavity (see Fig. 3): (i) radial (R), with a point defect of charge $k=+1$ at the center (positive winding number); (ii) polar (P), with two repulsive point defects of charge $k=+1/2$ located symmetrically with respect to the center of the cavity along one of its diameters; and (iii) uniform (U), with the director field more or less uniform. In the latter case the surface energy is not optimized, but elastic energy is low and there are no defects inside the cavity, whereas in the first two cases, R and P, the surface energy is minimized, but the fluid incurs an elastic free-energy cost and a contribution from defect-core energy. The U configuration may be considered as an extreme case of the P configuration, where the two defects are right at the surface at opposite ends. A further "escape" configuration, with an everywhere continuous director field, is only possible in (3D) cylindrical geometry, the escape direction being the cylinder axis. The relative stability of the R and P configurations will depend on the cavity radius R but also on the thermodynamic conditions and the material constants. Note that, contrary to the situation in 3D point defects [16,17], where the director may adopt a nonsingular biaxial configuration (e.g., by means of a ring disclination line), the defect cores are always isotropic here, which is the only possibility that avoids the director singularity.

The three possible configurations, R, P, and U, can be qualitatively described by means of a single parameter, d_0, defined as the distance between the two defects of Fig. 3(b). We then have $d_0=0$ for the R structure, $0<d_0<2R$ for the P
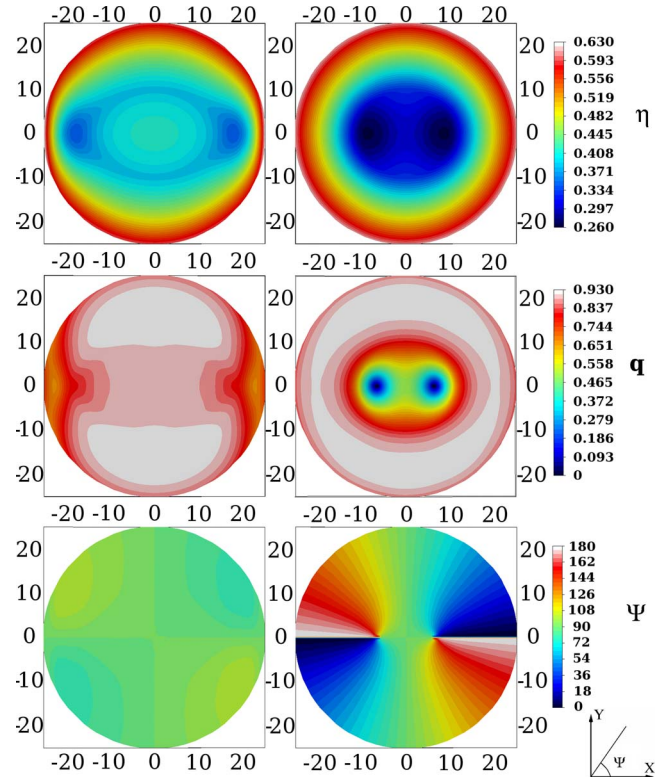

FIG. 4. (Color online) Contour plots with respect to xy coordinates for local packing fraction η (upper row), nematic order parameter q (middle), and director tilt angle Ψ (lower) for two configurations with the same grand potential in a cavity of radius $R=25.4D$ at relative chemical potential $\Delta\mu=2.75kT$. Left column corresponds to a U configuration, while right column is a P configuration. xy coordinates in units of D, and tilt angle is given in degrees.

structure, and $d_0=2R$ for the U configuration. Therefore, it what follows, we will use d_0 as the relevant structural quantity.

Our results indicate that, for small cavity radii R, there is a competition between two structures with different values of d_0. In Fig. 4 contour plots for local packing fraction η, nematic order parameter q, and tilt angle Ψ are shown for two structures that have the same value of cavity grand potential, $\hat{\Omega}$, for $R=25.4D$ and $\Delta\mu=2.75kT$ (here $\Delta\mu=\mu-\mu_0$ is the chemical-potential difference with respect to the bulk transition). From this figure one can interpret the two structures as corresponding to a U configuration (left column) and a P configuration (right column). In the U configuration the tilt angle Ψ is almost constant in the cell, and the only feature reminiscent of a defect is the slight modulation in order parameter. In general, density modulations are weak, except in the P configuration in a region surrounding both defects. The nematic order parameter is depleted in small, more or less circular, regions around each defect in the P state.

The locus of points in the $\Delta\mu-R$ plane where $\hat{\Omega}_U=\hat{\Omega}_P$ traces a curve which separates U and P configurations, with the U structure being favored for small cavity radii. The values of d_0 and $\langle q\rangle$ (average order parameter in the cavity) for the two structures, as a function of $\Delta\mu$, are plotted in Fig.
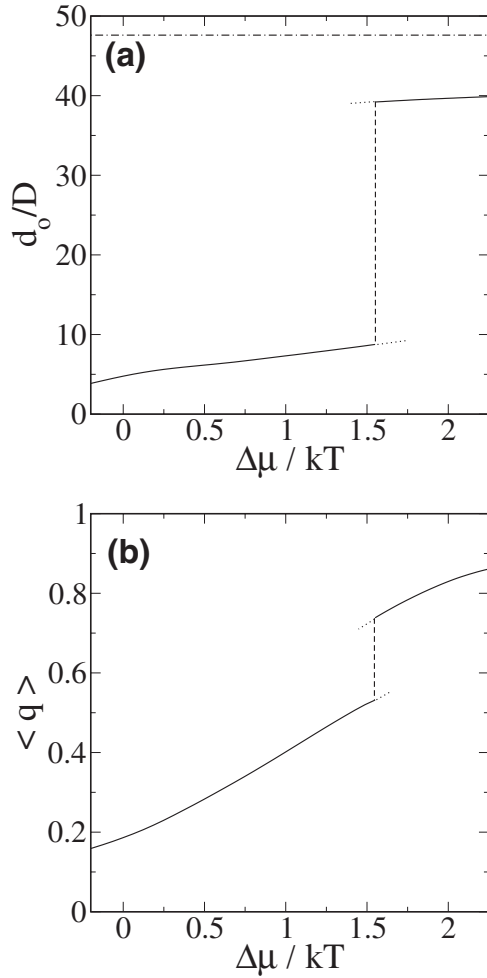
FIG. 5. (a) Defect separation d_0 as a function of relative chemical potential $\Delta\mu$ (with respect to value of bulk transition) for a nematic inside a cavity of radius $R=23.8D=1.49(L+D)$. (b) Average nematic order parameter in the cell $\langle q \rangle$ vs relative chemical potential for the same conditions. In both panels the dashed vertical lines indicate the location of the transition (using the criterion of equal cavity grand potentials), and the dotted lines correspond to metastable states. Dot-dashed line in (a) is the value of the cavity diameter.

5 for fixed R. As the chemical potential is increased from low values, i.e., from the P configuration close to the bulk value ($\Delta\mu=0$), defects increase their separation very slowly [Fig. 5(a)]. Suddenly, the defect separation jumps to a high value. There are metastable states in the P and U branches (dotted lines in the figure). The diameter of the cavity, $2R$, has been indicated by a horizontal dot-dashed line in the figure. We see that in the U configuration the defects are located at a distance less than one particle length from the surface (i.e., mesoscopically they are at the surface) and that this distance does not change much. In Fig. 5(b) the spatial average of the nematic order parameter over the cell is plotted. As expected, it increases with $\Delta\mu$. The transition from the P to the U states looks like a phase transition of the first order accompanied by discontinuities in the nematic order parameter. Since this is occurring in a finite system, it is only a pseudophase transition.
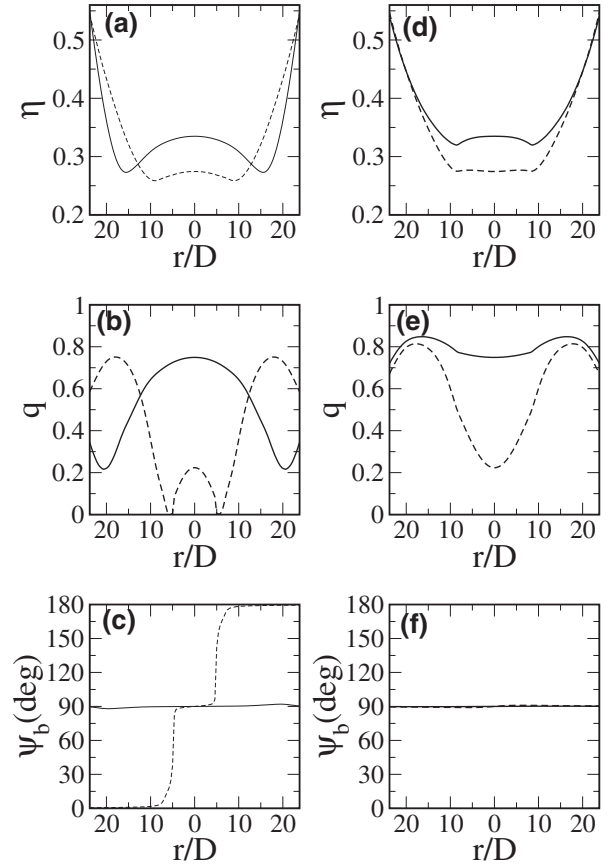

FIG. 6. Packing fraction η, nematic order parameter q, and tilt angle Ψ of the two configurations with the same grand potential in a cavity of radius $R=23.8D=1.49(L+D)$ at relative chemical potential $\Delta\mu=1.55kT$. Continuous lines: U configuration. Dashed lines: P configuration. [(a)–(c)] Path a and [(d)–(e)] path b, both as defined in Fig. 3(b).

Before proceeding further, it is necessary to discuss a point concerning the procedure used to minimize the free energy, specifically, how the initial configurations to initiate the conjugate-gradient procedure are chosen. The U configuration poses no problem, as configurations with constant values for density, order parameter and tilt angle quickly lead to minimum free-energy states. However, the P configuration contains two defects, and the positions of these defects are slow variables: finding the equilibrium state takes a lot of iterations to complete. In practice, we have performed partial minimizations at fixed defect separation d, which gives an effective free energy as a function of d. From this curve we locate the equilibrium value d_0 where the free energy is minimum and then perform a full minimization.

Figure 6 shows the profiles along the two cavity diameters indicated in Fig. 3(b). Panels (a)–(c) correspond to path "a," which goes along the diameter containing the two defects, while panels (d)–(f) refer to path "b," perpendicular to the previous one. Profiles of configurations U and P are indicated by continuous and dashed lines, respectively. The defect position is clearly visible in panel (b): the nematic order parameter goes to zero exactly at the defect center, which unequivocally determines its position. Note that in this case the order-parameter profile exhibits a maximum at a slightly
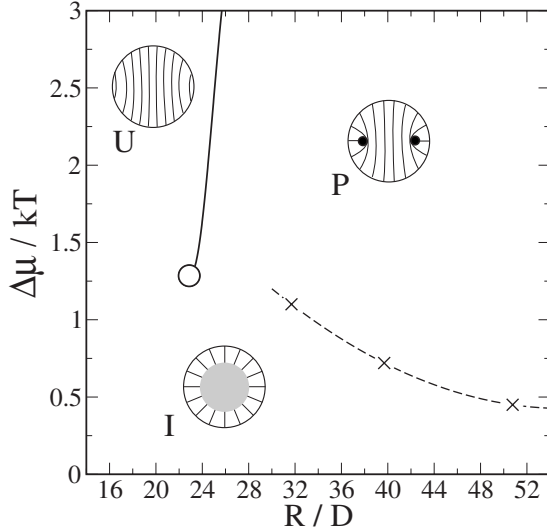
FIG. 7. Stability diagram in the plane relative chemical potential $\Delta\mu$ vs cavity radius R. Continuous line: $P-U$ transition line. Dashed line: curve defined by the inflection point of the $d_0(\Delta\mu)$ characteristic. Open circle: terminal point for $P-U$ transition line. Labels indicate the different stable configurations: P, polar; U, uniform; and I, isotropic phase. Schematic diagrams of director field in each configuration are also shown.

shifted position with respect to the surface (an effect already observed in density-functional [18] and MC studies [10] of three-dimensional model fluids subject to the same external potential).

By repeating the above procedure for different values of the cavity radius, a "phase diagram" (stability diagram) showing regions of stability of each configuration was constructed. This is shown in Fig. 7 in the chemical potential vs cavity radius plane. The continuous line indicates a transition line where the two structures have the same grand potential: the U phase, with $d_0 \simeq 2R$, stable for small cavities and the P phase, having $d_0 < 2R$, stable for the larger cavities. The slope of the transition line in the $\Delta\mu$-R plane is very high, which reflects the strongly structural character of the transition. However, the line ends in a terminal point at $R_c = 23.6D$ and $\Delta\mu_c = 1.36kT$, where the two configurations cannot be distinguished. At high chemical potential the simulations of Bates and Frenkel [15] predict a transition from the nematic to the crystal phase at packing fractions $\eta \simeq 0.8$, which are well above those shown in our figure. Therefore we expect that the $P-U$ transition be stable in a wide range of chemical potentials with respect to spatially ordered phases.

Our results are in agreement with those of Dzubiella *et al.* [9], who performed MC simulations on the same model fluid. The aspect ratios considered by these authors were $\chi = 16-21$, with cavity radii $R/L = 9-13$. In all cases they observed a stable phase with two defects of charge $k = +1/2$, which is in agreement with the present results. The MC simulations of Andrienko and Allen [10] on a fluid of hard ellipsoids of aspect ratio $\chi = 15$ confined in a (3D) cylindrical cavity also agree with our results. The external potential used by these authors was also the same as that studied here, and for all values of radius considered (2–5 particle lengths) they

found a stable configuration with two disclination lines of charge $k = +1/2$. It is interesting to note that the order-parameter profiles obtained by Andrienko and Allen are very smooth and do not present strong oscillatory behavior, a feature also present in our density-functional profiles. This gives some support to our approach, which does not use averaged densities of the type used in more elaborate density-functional theories for strongly inhomogeneous fluids of hard spheres, and may indicate that the highly frustrated state of the nematic inside the cavity induces smoother density and orientational distributions than what would otherwise correspond to such restricted geometries.

C. Analysis in terms of elastic theory

The $P-U$ transition found may be understood in the context of elastic theory [1]. Let us consider the two extreme cases $d_0 = 0$ (pure R state) and $d_0 = 2R$ (pure U state with no elastic deformation) and analyze their relative stability, assuming density and order parameter to be constant throughout the cell and equal to their bulk values. The excess free energy with respect to the bulk nematic has elastic, surface, and defect-core contributions. In the U configuration the only nonzero contribution is the surface contribution, which is optimized in the R configuration, but here the director field presents a pure splay deformation. In the latter the free energy is

$$F^R = \pi k_1 \log \frac{R}{r_n} - 2\pi b R + F_n^R, \qquad (15)$$

where k_1 is the splay elastic constant, r_n is the radius of the $k = +1$ defect core, F_n^R is its free energy, and $b > 0$ gives the surface contribution. For the U configuration

$$F^U = 2\pi a R, \quad a > 0. \qquad (16)$$

The difference in free energies is then

$$\Delta F = F^R - F^U = \pi k_1 \log \frac{R}{r_n} + F_n^R - 2\pi(a+b)R, \qquad (17)$$

which, assuming F_n and r_n to be constant with R, is always negative for large cavities since the elastic energy only grows logarithmically, i.e., the R phase is expected to be more stable. Depending on the type of surface and liquid crystal, it is plausible that, for small cavities, the free-energy balance can be inverted, and the U phase might become more stable.

In our density-functional model, the stable phase found is of the P, rather than R, type, i.e., the model predicts that it is more stable to create two $k = +1/2$ defects than a single $k = +1$ defect. In the simple theory, the elastic contribution of the P configuration is also logarithmic with the cavity radius, but it is half the value in the R configuration [19]:

$$F^P = \frac{\pi k_1}{2} \log \frac{R}{r_n} + F_n^P - 2\pi c R, \quad c > 0. \qquad (18)$$

The defect contribution F_n^P will include two core energies plus interaction energy between the two defects. The first is proportional to k^2 so that we expect it to be less than F_n^R by a factor of order 2, but there is repulsion between the $k =$
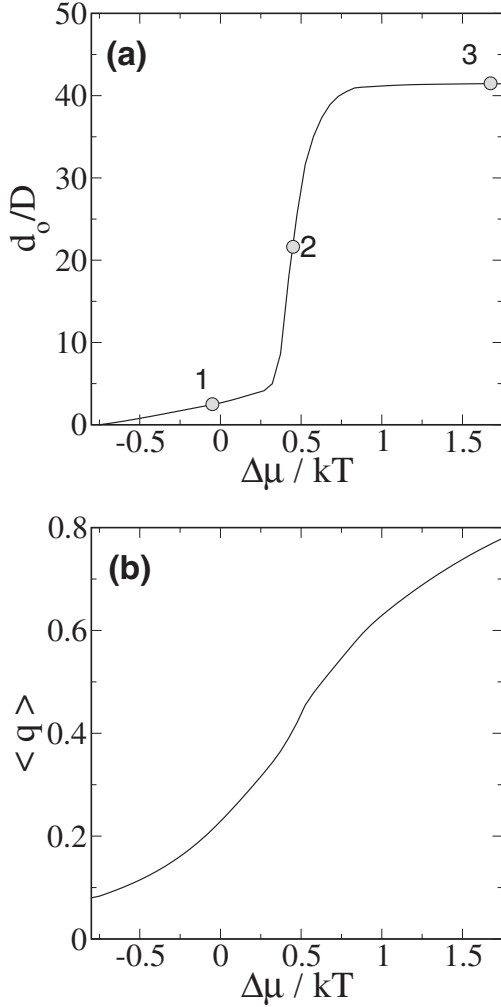
FIG. 8. (a) Defect separation d_0 as a function of relative chemical potential $\Delta\mu$ (with respect to value of bulk transition) for a nematic fluid inside a cavity of radius $R=50.77D=3.17(L+D)$. (b) Average nematic order parameter in the cell $\langle q \rangle$ vs relative chemical potential for the same conditions.

+1/2 defects, adding a positive contribution. Therefore, in the framework of elastic theory it is impossible to make predictions concerning the balance between the R and P configurations in small cavities, but for large cavities, where defect repulsion becomes less important, the P configuration is favored.

D. Separation between defects

In this section we consider the case where the cavity radius is large and, therefore, the P configuration is always stable. We will study how the separation between the two defects of charge $k=+1/2$ increases with chemical potential. In this regime no discontinuous change in d_0 occurs, but there are some features which are worth discussing.

Figure 8 illustrates a typical case, $R=3.17(L+D)$, which is approximately 2.1 times the value considered before (Fig. 5). We see, in panel (a), that d_0 first increases steadily (a typical point is 1), then very rapidly (point 2), i.e., defects separate very quickly, and finally d_0 levels off (point 3).

TABLE I. Equilibrium defect distance d_{eq} and surface-defect distance s for different cavity radii R.

R/D	$d_{eq}/2R$	s/R
50.8	0.41	0.59
63.7	0.39	0.61
95.7	0.39	0.61

Saturation settles at a value $d_{eq} \simeq 45D$, similar to the case represented in Fig. 5 but with the important difference that now the cavity diameter is $2R=101.54D$, and therefore, the defects are far from the surface: the corresponding distance is $s=R-d_{eq}/2=28.3D$. The average order parameter, panel (b), exhibits a smooth behavior with no discontinuity. The region at which defects separate quickly from each other occurs at chemical potentials closer to the bulk transition than in the previous case: $\Delta\mu=0.50kT$, to be compared with $\Delta\mu=1.55kT$ for $R=1.49(L+D)$.

On increasing the radius further, the saturation defect distance becomes larger. For example, for the same chemical potential, but with cavity diameter $2R=7.96(L+D)=127.4D$, the saturation value is $d_{eq} \simeq 53D$ so that $s=37.2D$. In the case $2R=191.4D$ we have $s=58.2D$. Clearly the equilibrium distance between the defects or the equilibrium distance between surface and defect is the result of a balance between the repulsive interaction between defects and the repulsive interaction between defect and surface, which are both long-ranged. For very large cavities it is plausible that an asymptotic distance would be reached although this regime we are not able to probe due to computational limitations.

An interesting observation is that the equilibrium defect distance d_{eq} or the surface-defect distance s, scale with R, the cavity radius. Table I summarizes the values found for the systems investigated. The lack of perfect scaling may be attributable to minor inaccuracies in the minimization with respect to d since small changes in d about the equilibrium value give rise to very small changes in the free energy.

Yan and Rey [20] analyzed a very similar system, but with discotic particles, and in the framework of elastic theory. They concluded that the defect separation scales with cavity diameter as $d_{eq}/2R=5^{-0.25} \simeq 0.67$, larger than our finding. However, the authors neglected the curvature of the surface and assumed the director distortions to be induced by mirror defects of opposite charge along the line joining the real defects (similar to the "method of images" in electrostatics), an approximation valid in the context of elastic theory. In addition, Yan and Rey used a uniform order parameter and a single elastic constant and neglected the defect core energy. These assumptions may be important when comparing with the density-functional results; in particular, the surface does certainly induce inhomogeneities in density and order parameter, and the curvature may somehow renormalize the scaling constant. Nevertheless, scaling seems to operate in both theories.

IV. RELATION WITH BULK TRANSITION

We have already shown the structural quantities in the P configuration when the cavity radius is small $R=1.49(L$
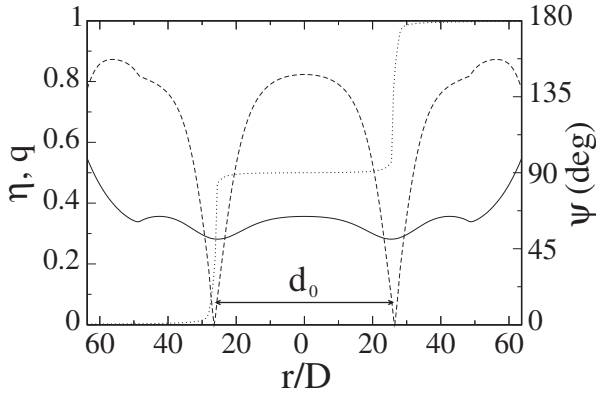
FIG. 9. Packing fraction η (continuous line), nematic order parameter q (dashed line), and tilt angle Ψ (dotted line) along path a [see Fig. 3(b)], for a fluid at $\Delta\mu=2.75kT$ inside a cavity of radius $R=63.7D=3.98(L+D)$.

$+D)$ (Fig. 6) and demonstrated that this structure is very smooth. This figure corresponds to a case where three density maxima along the defect diameter (path a) occur in the cavity, but another one is about to appear, which causes a broad central peak in density. The region between the two defects is a region with low orientational order, $q\simeq 0.2$.

Let us now examine the case $\Delta\mu=2.75kT$ but for a larger cavity, $2R=63.7D$. Figure 9 shows the structural quantities along the same path. Now in the region between the two defects the orientational order is high, $q\simeq 0.8$. The obvious conclusion is that the orientational order in the region between the defects is going to depend on d_0, which in turn depends on R and μ. Figure 10 contains the nematic order parameter for the three cases indicated in Fig. 8 as 1 (dotted line), 2 (dashed line), and 3 (continuous line). From these results it seems clear that the fast separation between defects is associated with a strong increase in order in the region between the defects. This, together with the fact that the value of μ at which the rapid increase in d_0 occurs approaches the bulk transition value as the radius becomes larger, leads to the obvious conclusion that the abrupt
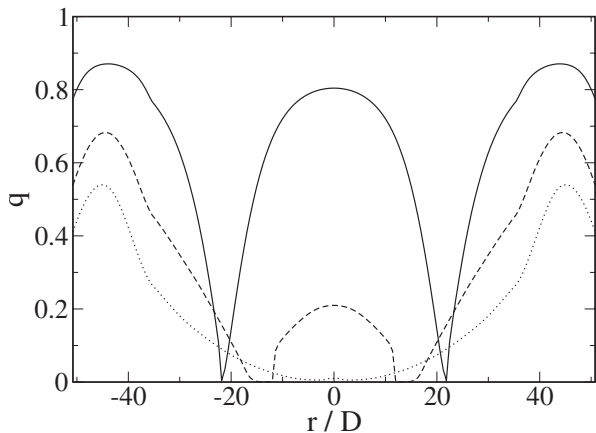

FIG. 10. Nematic order parameter along path a in Fig. 3 for a cavity of radius $R=50.77D=3.17(L+D)$ for three values of chemical potential: $\Delta\mu=-0.05kT$ (dotted line), $0.45kT$ (dashed line), and $1.67kT$ (continuous line).

changes are reminiscent of a isotropic-nematic transition. This "confined isotropic-nematic transition" is indicated in the stability diagram (Fig. 7) by a dashed line, separating the U configuration from a configuration with a large central region exhibiting orientational disorder (indicated in the diagram by the label "I"). The fact that this line has $\Delta\mu>0$ is to be expected, as the circular cavity tends to frustrate the order. This transition cannot be a true phase transition since it occurs in a system with confined geometry in all directions, i.e., in a truly finite system, which means that fluctuations (and consequently the phase transition) are suppressed altogether.

V. DISCUSSION AND CONCLUSIONS

The system studied, a fluid of elongated hard particles in a circular cavity, is subject to opposing fields that introduce frustration effects: the surface induces homeotropic orientation of the director field, but then the circular geometry demands the creation of point defects, i.e., defect-core and elastic free-energy contributions. The problem is similar [21] to the planar hybrid cell problem, consisting of two opposite surfaces that induce antagonistic orientations (say homeotropic and planar). In our case one of the surfaces is the cavity wall, while the other "surface" is the geometric center of the cavity. In the same way as in the planar hybrid cell, frustration may induce defective regions where the order parameter locally goes to zero, which optimizes surface energy while relaxing elastic strain, but this adds defect energy; the only way the fluid may get rid of this free-energy contribution is by adopting a uniform configuration, i.e., by not optimizing the surface energy contribution at the two surfaces simultaneously.

The interplay between the different configurations, i.e., the structural $P-U$ transition, affects and might in fact be related to the isotropic-nematic transition. In our present model this connection could not be established since there is no true phase transition due to the completely restricted geometry; however, there are traces of it, and a "ghost phase boundary" can be calculated. This boundary behaves like a frustrated transition line, i.e., confinement and frustration delays (and, strictly speaking, suppresses) complete nematization (cf. planar hybrid cell) in the cavity. The ghost phase boundary line could be somehow related to the structural transition (Fig. 7), a feature that should be studied more properly in a geometry where the transition actually exists as a true phase transition, for example, in cylindrical geometry. A related problem in 3D, where a disclination line induces nucleation of the isotropic phase, was discussed by Mottram and Sluckin [11].

As a final comment, we note that in the present calculations the chemical potential has been set deliberately to values close to the bulk isotropic-nematic transition in order to avoid the stabilization of phases with spatial order (i.e., the

crystal phase). A smectic phase does not appear to be stable in bulk [15] although a layered phase could be stabilized in a flat confined geometry (2D slit pore).

Obvious extensions of the present work include the evaluation of defect core energies and a detailed comparison with elastic energies, the extension to larger cavities, and the study of 3D problems. The latter system will demand a larger computational effort, but work along this line is already underway.

ACKNOWLEDGMENTS

[1] P. G. de Gennes and J. Prost, *The Physics of Liquid Crystals* (Oxford, New York, 1995).

[2] H. Kikuchi, H. Higuchi, Y. Haseba, and T. Iwata, SID Int. Symp. Digest Tech. Papers **38**, 1737 (2007).

[3] See, e.g., H.-R. Trebin, Liq. Cryst. **24**, 127 (1998).

[4] M. Kleman, Rep. Prog. Phys. **52**, 555 (1989).

[5] F. C. Frank, Discuss. Faraday Soc. **25**, 19 (1958).

[6] M. Svetec, S. Kralj, Z. Bradač, and S. Žumer, Eur. Phys. J. E. **20**, 71 (2006).

[7] C. Chiccoli, O. D. Lavrentovich, P. Pasini, and C. Zannoni, Phys. Rev. Lett. **79**, 4401 (1997).

[8] J. L. Billeter, A. M. Smondyrev, G. B. Loriot, and R. A. Pelcovits, Phys. Rev. E **60**, 6831 (1999).

[9] J. Dzubiella, M. Schmidt, and H. Löwen, Phys. Rev. E **62**, 5081 (2000).

[10] D. Andrienko and M. P. Allen, Phys. Rev. E **61**, 504 (2000).

[11] N. J. Mottram and T. J. Sluckin, Liq. Cryst. **27**, 1301 (2000).

[12] S. Kralj and S. Žumer, Phys. Rev. A **45**, 2461 (1992); Liq. Cryst. **15**, 521 (1993).

[13] M. Baus and J.-L. Colot, Phys. Rev. A **36**, 3912 (1987).

[14] T. L. Hill, *Thermodynamics of Small Systems* (Dover, New York, 1994).

[15] M. A. Bates and D. Frenkel, J. Chem. Phys. **112**, 10034 (2000).

[16] N. Schopohl and T. J. Sluckin, Phys. Rev. Lett. **59**, 2582 (1987).

[17] E. Penzenstadler and H.-R. Trebin, J. Phys. (Paris) **50**, 1027 (1989).

[18] D. de las Heras, L. Mederos, and E. Velasco, Phys. Rev. E **68**, 031709 (2003).

[19] M. Kleman and O. D. Lavrentovich, *Soft Matter Physics* (Springer, New York, 2003).

[20] J. Yan and A. D. Rey, Carbon **40**, 2647 (2002).

[21] P. Palffy-Muhoray, E. C. Gartland, and J. R. Kelly, Liq. Cryst. **16**, 713 (1994).